ELSEVIER

Journal of Fluids and Structures 26 (2010) 19–40

JOURNAL OF FLUIDS AND STRUCTURES

www.elsevier.com/locate/jfs

Vortex dynamics of a cylinder wake in proximity to a wall

S. Sarkar*, Sudipto Sarkar

Department of Mechanical Engineering, Indian Institute of Technology Kanpur, Kanpur 208016, India

Received 1 November 2008; accepted 13 August 2009
Available online 6 November 2009

Abstract

Large-eddy simulations (LES) are used to investigate the modifications of wake dynamics and turbulence characteristics behind a circular cylinder placed near a wall for varying gap-to-diameter (G/D) ratios (where G signifies the gap between the wall and the cylinder, and D the cylinder diameter). The three-dimensional (3-D), time-dependent, incompressible Navier–Stokes equations with a dynamic subgrid-scale model are solved using a symmetry-preserving finite-difference scheme of second-order spatial and temporal accuracy. The immersed boundary (IB) method is employed to impose the no-slip boundary condition on the cylinder surface. Flow visualizations along with turbulence statistics are presented to gain insight into the flow structures that are due to interaction between the shear layers and the approaching boundary layer. Apart from the vortex shedding mechanism, the paper illustrates the physics involving the shear layer transition, stretching, breakdown and turbulence generation, either qualitatively or quantitatively, in the presence of a wall for a Reynolds number of $\mathrm{Re} = 1440$ (based on D and the inlet free-stream velocity U_∞).

Keywords: Wake–boundary layer interactions; Shear layer transition; LES; IB method

1. Introduction

Flow around a cylinder in unbounded condition has been studied extensively for over a century because of its interesting flow features and practical applications as reflected in reviews by Roshko (1961), Berger and Willie (1972), Norberg (1994) and Williamson (1996). In contrast, the flow around a cylinder in presence of a wall has received less attention. However, this kind of study can directly be applied to many engineering problems, such as flow past a suspension bridge, pipelines near the ground, flow past building construction, heat transfer enhancement in heat exchangers, forced-air cooling of board-mounted electronic components, etc.

When the cylinder is placed close to a wall, the dynamics of vortex shedding changes appreciably. The cylinder is under the influence of a non-uniform velocity profile owing to the flow over a rigid wall, which has a non-symmetric influence on the body. This causes asymmetry in the strength of vortex shedding and generates a finite mean force directed away from the wall. Further, the vorticity shed from the cylinder interacts with the vorticity of the boundary layer resulting in an excited wake-induced boundary layer with complex flow structures. When the gap between the cylinder and the wall is relatively low, this nonlinear interaction is strong, provoking the separation of the boundary layer apart from a drastic change of the entire wake. Thus, the dynamics of vortex shedding in the presence of a wall is

*Corresponding author. Tel.: +91 512 2597942; fax: +91 512 2590007.
E-mail address: subra@iitk.ac.in (S. Sarkar).

0889-9746/$ - see front matter © 2009 Elsevier Ltd. All rights reserved.
doi:10.1016/j.jfluidstructs.2009.08.003

influenced by several factors, such as the approaching boundary layer thickness, free-stream disturbances, Reynolds number and gap between the cylinder and the wall. These factors also control the evolution of the boundary layer and its transition under excitation of the migrating wake. In brief, the major modifications of flow dynamics past a cylinder in the vicinity of a wall can be identified as: (i) deflection of the approaching boundary layer away from the wall, (ii) suppression of vortex shedding from the lower half of the cylinder, (iii) presence of separation bubble both upstream and downstream of the cylinder and (iv) a significant change of flow parameters such as Strouhal number, lift and drag coefficient.

The first significant experiment in this area was performed by Taneda (1965). A circular cylinder close to a wall was towed through the stagnant water at a low Reynolds number $\mathrm{Re} = 170$, where there was no effect of boundary layer. He observed a single row of vortices behind the cylinder for a small gap ratio of $G/D = 0.1$ and the wavelength of the vortices increased with downstream distance, which after a few wavelengths became unstable and broke down. As the gap ratio was increased to 0.6, a regular double row of vortices was re-established. Several experiments for the flow around a cylinder in the presence of a single plane boundary have been reported at moderately high Reynolds number, $\mathrm{Re} = 2 \times 10^4$ to 10^5 (Bearman and Zdravkovich, 1978; Grass et al., 1984; Taniguchi and Miyakoshi, 1990; Lei et al., 1999). In most of these cases, the approaching boundary layer was turbulent. The results illustrated that the aerodynamic forces on the cylinder were modified with a slight variation of the shedding frequency. The suppression of vortex shedding was observed when the body was closer than a critical distance from the wall, denoted by $(G/D)_{cr}$. This critical gap height was found to be approximately 0.3–0.4 (Bearman and Zdravkovich, 1978; Grass et al., 1984; Taniguchi and Miyakoshi, 1990; Buresti and Lanciotti, 1979). For smaller gaps, the wake was almost steady and the periodic shedding was strongly inhibited with separation bubbles on the wall. Later, Lei et al. (1999) reported that the suppression of vortex shedding occurred at a gap ratio of about 0.2–0.3 depending on the thickness of the approaching boundary layer.

As stated earlier, the magnitude of aerodynamic forces on the cylinder and the shedding frequency are altered in proximity to a wall. The frontal stagnation point moves towards the wall producing an upward lift (C_L) on the cylinder with the consequence of deviation of the wake away from the wall. This increases the base pressure, resulting in a low value of coefficient of drag (C_D), although these depend on the boundary layer, its character and thickness. The drag coefficient remained largely unaffected by G/D when the cylinder was placed outside the boundary layer (Lei et al., 1999; Zdravkovich, 1985). As the cylinder was moved into the boundary layer, C_D decreased with G/δ (where δ is the thickness of the boundary layer). However, Buresti and Lanciotti (1979) argued that there was hardly any correlation between C_D and G/δ. Taniguchi and Miyakoshi (1990) and Lei et al. (1999) observed that when the lower surface of the cylinder was placed within the critical gap ratio, the r.m.s. values of both lift (C'_L) and drag (C'_D) coefficients strongly reduced. This might be attributed to the diffusion of velocity fluctuations because of the boundary layer. Regarding the vortex shedding frequency (Strouhal number, St), Angrilli et al. (1982) found an influence of gap ratio on St if G/D was less than 5.0, where Re was in the range of 2.8×10^3–7.6×10^3. However, others (Bearman and Zdravkovich, 1978; Grass et al., 1984; Zdravkovich, 1985; Taniguchi and Miyakoshi, 1990) observed that the shedding frequency was almost independent of gap ratio. A possible reason for this difference was the different range of Re used in the experiment of Angrilli et al. (1982) as compared to others. Furthermore, the study of Lei et al. (1999) indicated that the velocity gradient apart from the gap ratio also influenced the shedding frequency. The increase of St with reduction of G/D could only be felt for a thinner boundary layer, whereas no significant change was observed for a thicker boundary layer.

The flow visualization around a circular cylinder near a wall was performed by Price et al. (2002) for Re between 1200 and 4960 and G/D between 0 and 2. They concluded that the G/D ratio was a major factor for the change of flow characteristics. The flow interactions between cylinder wake and flat plate boundary layer have been divided in four zones based on the G/D ratio. For $G/D < 0.125$, the flow beneath the cylinder was suppressed and separation of boundary layer occurred both upstream and downstream of the cylinder. Although there was no regular vortex shedding, a periodicity associated with the outer shear layer was found. For $0.25 < G/D < 0.375$, the separation region decreased, but the flow characteristics were the same as those of the previous case. A pronounced pairing between the inner shear layer shed from the cylinder and the wall boundary layer was observed in this case. For $0.5 < G/D < 0.75$, the vortex shedding started and for $G/D > 1.0$ there was no separation of the wall boundary layer either upstream or downstream of the cylinder. They observed that the variation of St with gap ratio was mainly dependent on Re. For low Reynolds number flows ($\mathrm{Re} < 2600$), St was significantly greater than that of an isolated cylinder for $G/D < 2$. But as Re was increased ($\mathrm{Re} > 4000$), St became insensitive to the G/D ratio. The paper presented the flow interactions with the help of instantaneous vorticity and power spectra.

Numerical simulation of flow past a cylinder in the vicinity of flat plate is very limited. It was first performed by Vada et al. (1989) using vortex in cell method for transcritical Reynolds number, $\mathrm{Re} = 3.6 \times 10^6$ and $G/D = 0.4$, 0.8 and 1.5. They observed the appearance of mean lift force and increased drag due to the presence of a wall. The simulation

suffered from over-prediction of drag coefficient and under-prediction of lift coefficient as compared to the experiment of Zdravkovich (1985) for a small gap ratio. Liou et al. (2002) performed a LES of the turbulent wake in proximity to a wall for a $Re = 2.2 \times 10^4$, although a square cylinder was considered and the discussion was focused on the phase-averaged vortex dynamics. The celerity of the positive vortex shed from the lower side of the cylinder was smaller than that of the upper side shed vortex due to the interaction with the boundary layer. Recently, Dipankar and Sengupta (2005) solved the cylinder boundary layer interaction considering two-dimensional $\psi-\omega$ formulation. They have tried to mimic the experiment of Price et al. (2002) considering $Re = 1200$ and $G/D = 0.5$ and 1.5. The computation illustrated larger vortical structures as compared to the experiment with rollup of vortices closer to the cylinder and failed to capture the breakdown. This was attributed to the fact that the absence of spanwise direction in 2-D simulation failed to redistribute the energy in the third direction, developing unrealistic large structures (Mittal and Balachandar, 1995).

The present paper will focus on the characteristics of the vortex shedding and its modifications behind a cylinder as the wall is approached for a Reynolds number in the shear layer transition regime. Although there are experimental investigations illustrating the vortex shedding process as well as the aerodynamic forces on the cylinder in proximity to a wall, the physics of flow including the shear layer stretching, breakdown and turbulence generation are not very complete. Most of the numerical simulations made so far on this flow configuration are in two-dimensional framework and thus elucidate the flow characteristics with limited success, particularly for high Reynolds numbers. An appropriate numerical tool in 3-D computational environment is very much needed for a complete study of the vortex dynamics and turbulence characteristics. It should be noted that in complex turbulent flows, where an understanding of the eddy motions and their interactions is the key to comprehension of the flow, a LES is often considered as an alternate root of DNS because of its economy. Considering all these factors, a 3-D LES with a dynamic subgrid-scale model has been used to investigate the flow around a cylinder near a wall at $Re = 1440$ and for G/D of 0.25, 0.5 and 1.0. Here, the wake dynamics and its nonlinear interactions with the approaching boundary layer involving the large- and small-scale structures are illustrated. The present paper is organized as follows. We describe the governing equations, geometrical configuration followed by flow validation and grid resolution study. Next we present the results and discuss the flow physics with the help of instantaneous flow visualization along with the turbulence statistics. Finally, we end the paper with a concluding note.

2. Numerical methods

2.1. Governing equations

In the present study, we perform LES of incompressible flow. The filtered mass and momentum equations can be expressed as

$$\frac{\partial \bar{u}_j}{\partial x_j} = 0, \tag{1}$$

$$\frac{\partial \bar{u}_i}{\partial t} + \frac{\partial}{\partial x_j}(\bar{u}_j \bar{u}_i) = -\frac{1}{\rho}\frac{\partial \bar{P}}{\partial x_i} + \frac{1}{Re}\nabla^2 \bar{u}_i - \frac{\partial \tau_{ij}}{\partial x_j} + \bar{f}_i, \tag{2}$$

where $\overline{u_i}$ denotes the filtered velocity field and $\tau_{ij} = \overline{u_i u_j} - \bar{u}_i \bar{u}_j$is the residual stress tensor (also known as subgrid-scale stress, SGS). The presence of the body forces $\overline{f_i}$ is due to the IB method, which will be discussed later. The above equations have been made dimensionless using the inlet free-stream velocity U_∞ and the cylinder diameter D. The resulting Reynolds number is defined as $Re = U_\infty D/\nu$, ν being the kinematic viscosity. The model proposed by Germano et al. (1991) and modified by Lilly (1992) is used here to include the effect of subgrid motions in the resolved LES, where the model coefficient C is dynamically calculated instead of input *a priori*. The least-squares estimate of the optimal solution for C, following Lilly, is employed by averaging over the homogeneous z-direction. Thus, the resulting C is the function of time and the inhomogeneous coordinates x and y. No damping of the turbulent viscosity, such as the one proposed by van Driest, is applied as solid walls are approached. The momentum advancement is explicit using the second-order Adams–Bashforth scheme, except for the pressure term, which is solved by a standard projection method. The pressure equation is discrete Fourier transformed in one dimension (in which the flow can be considered homogeneous and hence periodicity of flow can be imposed) and is solved by the BI-CG algorithm (Zhang, 1997) in the other two dimensions. The spatial discretization is second-order accurate on a staggered mesh arrangement using a symmetry-preserving central-difference scheme, which is widely used in LES owing to its non-dissipative and

conservative property (Mittal and Moin, 1997; Morinishi et al., 1998). However, as an alternative to the classical LES, implicit LES methods have been proposed in recent years relating the dispersion and dissipation with turbulence properties to encompass the constraints in near-wall flows (Drikakis, 2003).

Here, the simulations of flow past a cylinder in proximity of a wall have been performed in the Cartesian grid considering the origin of axes lies on the flat plate and at a distance of $10D$ from the leading edge. The coordinates x, y, z denote the streamwise, wall-normal and spanwise directions, respectively, and the corresponding velocities are denoted by u, v and w. The computational domain and boundary conditions used here are illustrated in Fig. 1. The domain extends from $-5D$ at the inflow to $25D$ at the outflow with a spanwise length of $3D$. It should be noted that a spanwise length of πD was used by Beaudan and Moin (1994), Mittal and Moin (1997) and Kravchenko and Moin (2000) while simulating the flow around a circular cylinder in unbounded condition for $\mathrm{Re} = 3900$ (the shear layer transition region). It was also reported that doubling the domain in the spanwise direction did not affect the results significantly (Kravchenko and Moin, 2000). The instant spanwise length of $3D$ appears reasonable in spite of an influence of Reynolds number scaling.

A Blasius profile is imposed at the inlet considering the computational domain begins at a $5D$ distance downstream from the leading edge of the flat plate, where the boundary layer thickness is considered as $0.295D$. A non-reflecting boundary condition (Orlanski 1976) is applied at the exit. The no-slip boundary condition ($u = v = w = 0$) is applied on the flat plate and on the cylinder surface. A free-slip velocity ($v = 0$, $\partial u/\partial y = \partial w/\partial y = 0$) is imposed along the upper surface of the domain, which does not allow outflow through the top surface. This causes the flow to accelerate above the boundary layer in order to compensate for the growth of the boundary layer. In the spanwise direction, the periodic boundary condition is used.

The IB method helps to impose boundary conditions on a given surface not coinciding with the computational grid as in the present case. Thus, to satisfy the no-slip boundary conditions at the cylinder surface, the IB technique is employed following Fadlun et al. (2000), which belongs to the class of 'direct forcing method'. The velocity field near the boundary of the body is modified at each step in such a way that the no-slip boundary condition is satisfied on the surface. This is done using some interpolations, which is equivalent to including a body force $\overline{f_i}$ in the momentum equation. In this paper, a quadratic unidirectional interpolation by Muldoon and Acharya (2005) is used. The flow solver has been extensively validated for a variety of transitional and turbulent flows (Sarkar and Voke, 2006; Sarkar, 2007, 2008) including simulation of vortex dynamics behind a circular cylinder for a wide range of Reynolds numbers (Sarkar. and Sarkar, 2007a b).

2.2. Computational details

The LES of flow past a circular cylinder near a wall is performed at a $\mathrm{Re} = 1440$ and for three gap ratios, $G/D = 0.25$, 0.5 and 1.0 following the experiment of Price et al. (2002). In the streamwise direction, a uniform and refined mesh is used near the cylinder to get adequate immersed-boundary points on the cylinder surface. Away from the cylinder, the mesh is slowly stretched out. In the flow-normal direction, a refined and uniform mesh is employed near the wall (up to $y/D = 2$ for $G/D = 0.25$, 0.5 and $y/D = 2.5$ for $G/D = 1.0$) to resolve the wake behind the cylinder and its interaction with the boundary layer. A uniform mesh is used in the spanwise direction owing to the symmetry of the body.

The evolution of boundary layer excited by the wake depends on a realistic representation of wake structures behind a cylinder. To estimate the resolution in the vicinity of a cylinder, we first performed LES of flow past a cylinder in an

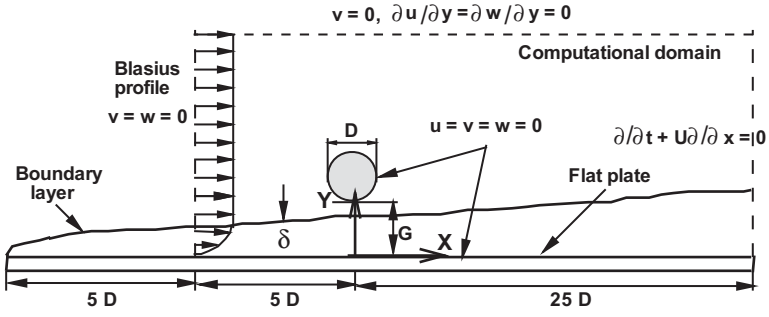

Fig. 1. Schematic diagram of the computational domain with the boundary conditions.

unbounded condition for two Reynolds numbers, Re = 1000 and 3900. Here, the computational domain extends from $-8.25D$ at the inflow to $25.75D$ at the outflow and from $-8.25D$ to $8.25D$ in the cross-flow direction with a spanwise length of $3D$. A mesh of $360 \times 192 \times 32$ points is used for Re = 1000, while a mesh of $384 \times 204 \times 32$ points is used for Re = 3900. For Re = 1000, among 360 streamwise grid points, 64 points are distributed upstream of the cylinder ($-8.25D$ to $-0.75D$), 64 points within $-0.75D$ to $+0.75D$, 150 points in the near wake ($+0.75D$ to $+10.75D$) and rest are distributed in the far field downstream, whereas for Re = 3900 the grid distributions are 64, 76, 150 and 82 in the respective regions. The spacing between adjacent grid points near the cylinder becomes $0.0156D$ for Re = 1000 and $0.013D$ for Re = 3900. Ovchinnikov et al. (2006) illustrated that a grid spacing of $0.015D$ near the cylinder was adequate to resolve flow in the wake for Re = 3900, where a LES with the IB method was used. However, the near-wall mesh distributions used here accommodate limited points within the laminar boundary layer on the windward side of the cylinder (according to the boundary layer theory, Schlichting 1979). For Re = 3900, a total of 146 IB-points for u-velocity along the cylinder surface are obtained by the grid distribution as compared to 140 surface points used by Mittal and Moin (1997) for a LES at the same Re. In the near wake region, non-dimensional mesh spacing varies as $\Delta x^+ = 0.1-3.5$, $\Delta y^+ = 0.05-1.8$, $\Delta z^+ = 0.1-2.9$. The mean values of Δx^+, Δy^+ and Δz^+ over a range of $x/D = 1$–25 along the cylinder axis of the cylinder are 1.4, 0.3 and 1.7, respectively.

Fig. 2 depicts the mean velocity profiles obtained at three different sections ($x/D = 3$, 5, 7) for Re = 1000, which is the lower limit of the shear layer transition according to Williamson (1996). The velocities are normalized by the maximum mean velocity deficit $\bar{u}_{\mathrm{wake,max}}$ and the lengths are normalized by the wake half-width b, which is defined as the distance between two points at which the mean velocity deficit becomes half of $\bar{u}_{\mathrm{wake,max}}$. The normalized mean velocity profiles obtained from three different locations collapse almost to a single curve, which is in good agreement with experimental measurements and data correlations of Schlichting (1979), i.e., $\bar{u}_{\mathrm{wake}}/\bar{u}_{\mathrm{wake,max}} = [1 - (\bar{y}_{\mathrm{wake}}/1.1338b)^{1.5}]^2$. This demonstrates that the simulated wake has reached a self-similar state.

For Re = 3900, the mean streamwise velocity profiles from the present simulation are compared with the experimental data of Lourenco and Shih [data taken from Ma et al. (2000)] for the very near wake region ($x/D \leq 3$) and the data of Ong and Wallace (1996) for the vortex shedding region ($x/D = 4$ and 7) in Fig. 3. It is interesting to note that velocity profiles agree well with the experimental data resolving a V-shaped profile in the recirculation region immediately behind the cylinder at $x/D = 1.06$ and 1.54. The streamwise velocity profile tends to attain a U-shape downstream of the recirculation region, at $x/D = 2.02$. The U-shaped profile in the vortex shedding region ($x/D = 4$, 7) may be attributed to the development of turbulence and enhanced mixing. The turbulence statistics (not shown) obtained from the present LES are also in fair agreement with the experimental data of Ong and Wallace and DNS of Ma et al. (2000). The study illustrates that the grid resolution chosen is good enough to predict the physics of the flow past a cylinder, e.g. flow structure in the near wake and the shear layer transition downstream.

In order to ensure the accuracy of calculations for the wake and boundary layer interactions, a grid resolution test has been carried out for a gap ratio of $G/D = 0.25$. The grid requirements to resolve the transitional flow or the boundary layer excited by external disturbances, such as in the present case, are less well established. However, the grid requirements for the simulation of fully turbulent boundary layer using a second-order accurate LES solver are well known ($\Delta x^+ \simeq 50$, $\Delta y^+_{\mathrm{min}} < 1.0$ and $\Delta z^+ \simeq 20$). Jacobs and Durbin (2001) indicated that the prediction of boundary layer

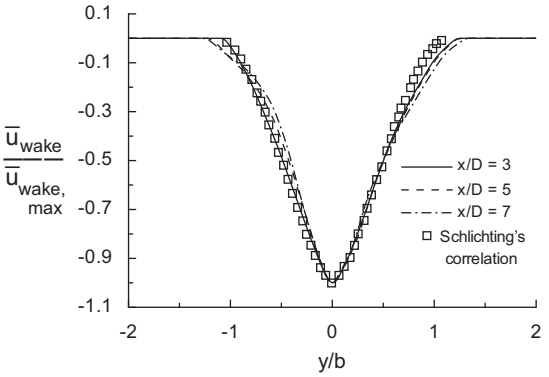

Fig. 2. The wake deficit for flow over a circular cylinder at Re = 1000.

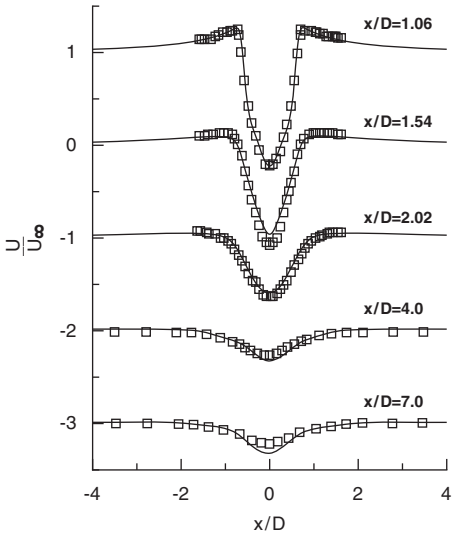

Fig. 3. Time averaged streamwise velocity at different x/D locations for flow over a circular cylinder at $\mathrm{Re} = 3900$: ——, present computation; □, experimental results.

transition is sensitive to streamwise resolution. Further, Ovchinnikov et al. (2006) illustrated that an under-resolved calculation predicts a premature and abrupt transition. In the present computation, four levels of mesh, such as $288 \times 192 \times 32$, $384 \times 160 \times 32$, $384 \times 192 \times 32$ and $384 \times 192 \times 64$ (designated as grid 1, grid 2, grid 3 and grid 4) in the streamwise, wall-normal and spanwise directions, respectively, are used. For grid 1, among 288 streamwise grid points, 32 points are distributed upstream of the cylinder ($-5D$ to $-D$), 96 points surrounding the cylinder ($-D$ to $+D$), 108 points near wake region ($+D$ to $+10D$) and the rest are distributed in the far field downstream ($+10D$ to $+25D$), whereas for other three mesh levels (384 points), the distribution is 40, 96, 160 and 88 in the respective regions. In the wall-normal direction, a total of 128 grid points with equal spacing are used between 0 to $2D$ and remaining 64 points are slowly stretched away from the cylinder ($+2D$ to $+8.5D$) for grid levels 1, 3 and 4. For grid 2, the distribution is 96 and 64 in the respective regions. The grid resolution near the cylinder is almost the same as used for the LES in the unbounded condition at $\mathrm{Re} = 1000$. It should be noted that the boundary layer thickness assuming a laminar flow at the location of cylinder without its presence is $0.42D$ and approximately 27 grid points are employed within the boundary layer for grid 3.

The profiles of mean ($\overline{U}/U_\infty$) and r.m.s. ($u_{\mathrm{rms}}/U_\infty$) streamwise velocity at $x/D = 2$, 3, 5, 7, 10 and 15 are depicted in Fig. 4 for all four grid levels. The data are normalized by the free-stream velocity and the cylinder diameter. No significant differences in the mean velocity profiles are observed between grid 1 and grid 4 except at $x/D = 3$ (Fig. 4(a)): the location of breaking down of shear layers to smaller eddies for $G/D = 0.25$. However, u_{rms} profiles exhibit appreciable differences between grid levels 1 and 4 (Fig. 4(b)). This indicates that there is a need of large number of grid points in the near wake region and inside the boundary layer. For the subsequent analysis, grid 3 is chosen considering the fact that there were no considerable changes of both the mean and r.m.s. velocity profiles by further increasing the grid points. In the near wake ($x/D = 3$–15) region, non-dimensional mesh spacing for grid 3 varies as $\Delta x^+ = 0.15$–15, $\Delta y^+ = 0.07$–1.5, $\Delta z^+ = 0.1$–7.5. For $G/D = 0.5$, the same computational domain and grid distribution are used as considered in $G/D = 0.25$. The computational domain is extended by $0.5D$ in the wall-normal direction for $G/D = 1$ (to assure almost a similar free-stream condition) keeping the streamwise domain unchanged. Here, a total of 160 grid points with equal spacing are used between 0 and $2.5D$ and 64 grid points are distributed in the remaining ($+2.5D$ to $+9D$) normal direction. Few parameters such as the domain, grid distributions and the values of Δx^+, Δy^+ and Δz^+ averaged between $x/D = 3$ and 15 are summarized in Table 1 for different cases.

The time step was about $\Delta t = 1.125 \times 10^{-3}(D/U_\infty)$ in nondimensional units. This time kept the Courant number below 0.2 for the entire simulation and the viscous stability number was much less. The flow field was allowed to evolve for 15 vortex shedding cycles to get a dynamically steady state solution. Then the data were collected for statistics for a period of 15 cycles that was found sufficient to ensure statistically converged results.

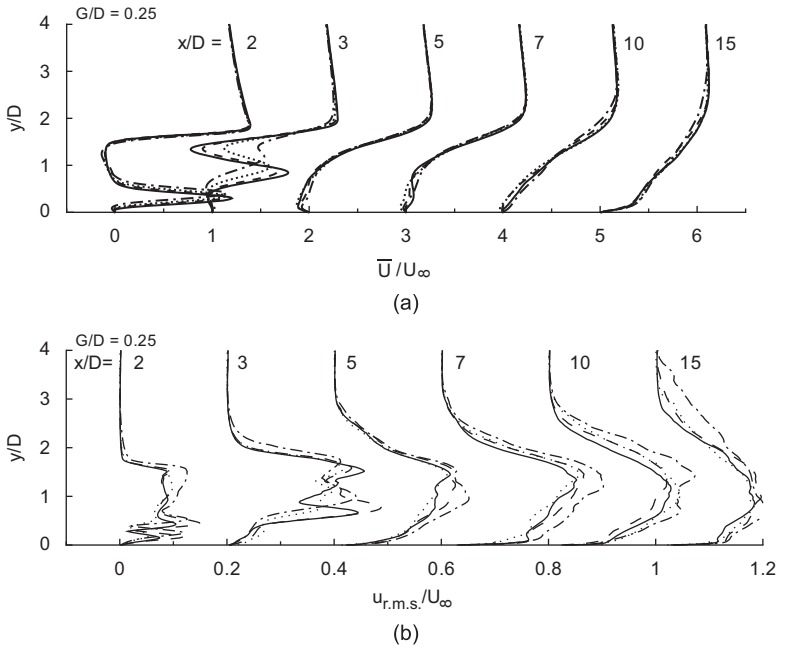

Fig. 4. Grid-independent test for $G/D = 0.25$ and $\mathrm{Re} = 1440$ considering (a) mean streamline velocity ($\overline{U}/U_\infty$) and (b) r.m.s. of streamline velocity (u_{rms}/U_∞) profiles at $x/D = 2$, 3, 5, 7, 10 and 15: –·–·–, $288 \times 192 \times 32$ (grid 1); –·–·–, $384 \times 160 \times 32$ (grid 2); ——, $384 \times 192 \times 32$ (grid 3); · · · · · · · · ·, $384 \times 192 \times 64$ (grid 4).

Table 1
Computational grid and box size.

G/D	Dimension of box ($L_x \times L_y \times L_z$)	Grid ($n_x \times n_y \times n_z$)	Δx^+	Δy^+	Δz^+	Comments
0.25	$30D \times 8.5D \times 3D$	$288 \times 192 \times 32$(grid 1)	7.96	0.68	4.11	Test case
		$384 \times 160 \times 32$(grid 2)	3.82	0.86	3.85	Test case
		$384 \times 192 \times 32$(grid 3)	4.35	0.71	4.41	Used
		$384 \times 192 \times 64$(grid 4)	4.23	0.74	2.25	Test case
0.5	$30D \times 8.5D \times 3D$	$384 \times 192 \times 32$	4.07	0.68	4.12	Used
1.0	$30D \times 9D \times 3D$	$384 \times 224 \times 32$	4.87	0.8	4.93	Used

3. Results and discussion

3.1. Time-averaged flow features

The modifications of wake dynamics behind a circular cylinder in the presence of a nearby boundary layer are discussed in this section. Fig. 5 presents the iso-contours of time-averaged streamwise velocity along with a few selected streamlines for the three gap ratios. When the cylinder is very close to the wall ($G/D = 0.25$), the shear layers remain frozen for a considerable time before they curl up to form the Kármán rolls, and these rolls lost their symmetry because of suppression of vortex shedding. The front stagnation point moves towards the wall from the centreline of the cylinder. Furthermore, the inner separation point shifts downstream along the shoulder of the lower half of the cylinder, while the outer separation point moves upstream along the shoulder of the upper half that changes the wake size behind the cylinder. The deflection of the wake and its departure from symmetry due to the wall proximity can be understood by the iso-contours of streamwise velocity. Further, a strong coupling between the inner shear layer and the boundary layer in this case accentuates the deflection of the boundary layer away from the wall forming a large downstream separation (which is designated as the primary bubble). A secondary bubble rotating in the opposite direction is formed beneath the primary bubble. The mean streamlines also depict the formation of an upstream separation for the low gap

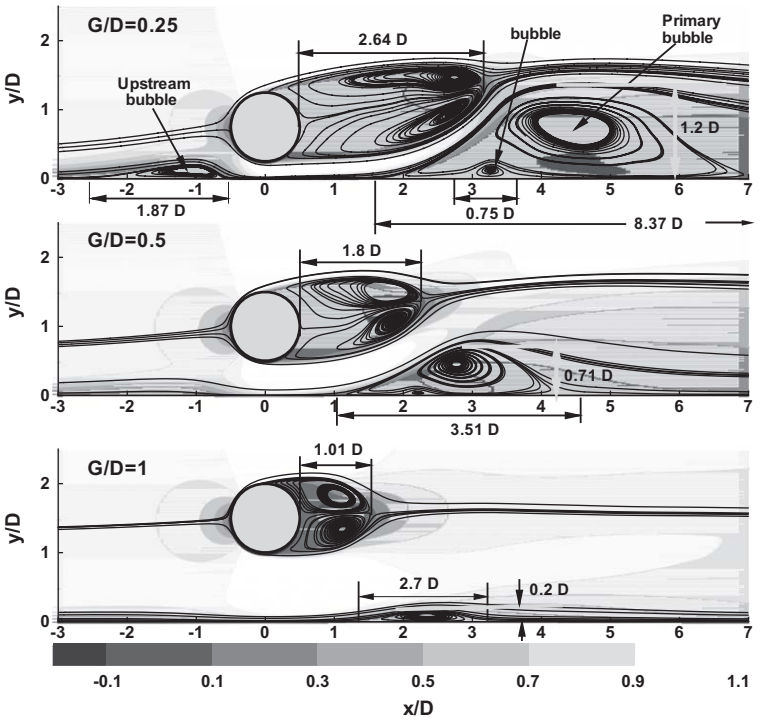

Fig. 5. Mean streamwise velocity contours along with few selected streamlines for different gap ratios.

ratio. As the gap ratio increases, the downstream separation bubble rapidly reduces and the upstream separation region disappears. Moreover, the Kármán rolls from the curling of the inner and outer shear layer form closer to the cylinder and appear symmetrical. The bubble length and its height along with the recirculation length of the shear layers are marked in the figure. For an increased gap ratio ($G/D = 1$), the recirculation length of the shear layer becomes $1.01D$, which approaches the value of recirculation length of flow past a circular cylinder in an unbounded condition (a recirculation length of 0.93 is seen at $\mathrm{Re} = 1000$ in the present simulation). The deflection of the boundary layer is also inhibited as compared to previous cases. The front stagnation points determined from the present LES are approximately at $\theta_S = -10.6^\circ$, -9.0° and -4.9° for $G/D = 0.25$, 0.5 and 1.0, respectively, where θ_S is measured from the front point on the horizontal axis of the cylinder and in the clockwise direction. The variation of θ_S fairly agrees with the experiment of Lei et al. (1999), where θ_S were -9.6°, -6.8° and -3.3° for $G/D = 0.3$, 0.5 and 1.0, respectively, at $\mathrm{Re} = 1.30{-}1.45 \times 10^4$ and boundary layer thickness $\delta/D = 0.48$. It should be noted that in our case $\delta/D = 0.42$, but $\mathrm{Re} = 1.44 \times 10^3$.

The lift coefficient (C_L), drag coefficient (C_D) and Strouhal frequency (St) are three non-dimensional parameters, which are helpful to describe the effects of boundary layer on the wake dynamics. As the cylinder is moved towards the wall, the mean lift coefficient ($\overline{C_L}$) becomes positive with decrease of $\overline{C_D}$. The movement of the frontal stagnation point towards the wall is associated with the generation of an upward lift, while the movements of separation points with an increase of the base pressure result in a reduced drag coefficient. The lower shear layer of the cylinder is suppressed because of the wall boundary layer, which also affects the base pressure. Thus, both the G/D ratio and the boundary layer thickness influence the aerodynamic forces on the cylinder. The present LES predicts a value of $\overline{C_L}$ as 0.124 and a value of $\overline{C_D}$ as 0.90 for a low gap ratio, $G/D = 0.25$, which appears to be below the critical gap ratio (highly correlated to the boundary layer thickness). As the gap ratio is increased to 1.0, $\overline{C_L}$ approaches zero with a value of 0.0075, while $\overline{C_D}$ becomes 1.47. A similar trend in the variations of $\overline{C_L}$ and $\overline{C_D}$ was reported by Lei et al. (1999) and Zovatto and Pedrizzetti (2001), although the magnitude was different because of differences in Reynolds number, the boundary layer thickness and its character. Furthermore, the r.m.s. values of C_L obtained from the LES are 0.008 and 0.27 for $G/D = 0.25$ and 1.0, respectively. The reduced r.m.s. value also confirms that the vortex shedding is suppressed at $G/D = 0.25$. Above the critical gap ratio, the regular vortex shedding abruptly starts to develop that rapidly changes the r.m.s. values (Taniguchi and Miyakoshi, 1990; Lei et al., 1999).

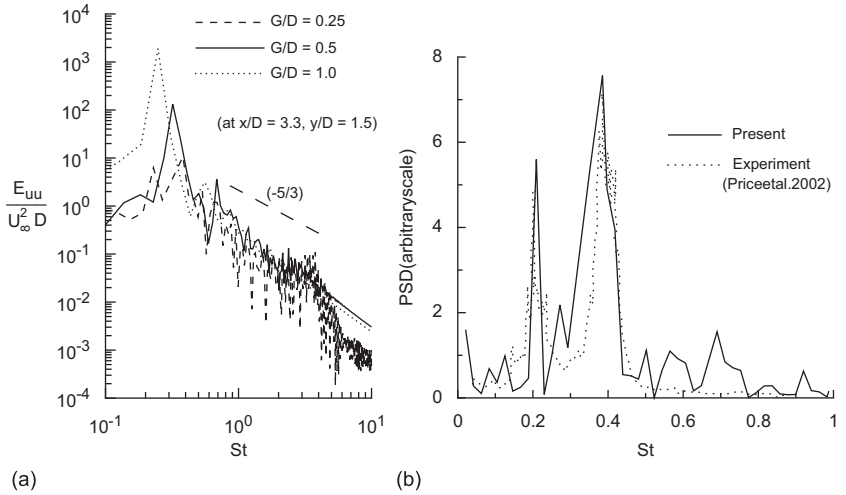

Fig. 6. Power spectra density of streamwise velocity at $x/D = 3.3$, $y/D = 1.5$ for Re = 1440: (a) for all gap ratios; (b) a zoomed view comparing with experiment for $G/D = 0.25$.

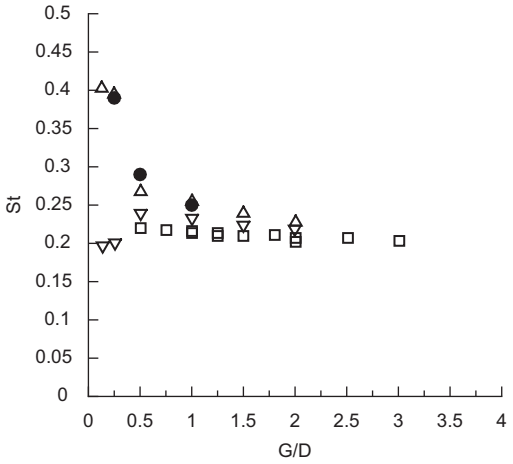

Fig. 7. St plot for different G/D ratios: ●, present LES (Re = 1440); △, Price et al. (Re = 1900); ▽, Price et al. (Re = 4900); □, Angrilli et al. (Re = 2860, 3820, 7640).

From the mean flow particularly at a low gap ratio, it is difficult to appreciate the vortex shedding. However, there exists a strong periodicity component to the predicted velocity signal in the cylinder wake; almost certainly, this is associated with the shear layer shed from the outer surface of the cylinder. A spectral analysis is performed after collecting the velocity histories in the mid-span plane at a location of $x/D = 3.3$ and $y/D = 1.5$ from the cylinder center over a time period of $TU_\infty/D = 15$ (T being the time period of vortex shedding). Fig. 6(a) depicts the power spectra of the streamwise velocity fluctuations for all the gap ratios. This reveals that as the cylinder approaches the wall, the Strouhal frequency increases due to the suppression of vortex shedding. For a low gap ratio ($G/D = 0.25$), a dominant wake frequency occurs at St = 0.4; however, there is also a secondary peak at St = 0.23. These two peaks are attributed to the difference in celerity of the positive vortex shed from the lower side of the cylinder than that of the negative vortex shed from the upper side: result of the vortex-boundary layer interactions. The prominent shedding frequency shifts to 0.29 and 0.25 for $G/D = 0.5$ and 1.0, respectively. Furthermore, the power spectra illustrate that the effect of the wall boundary layer reduces as the gap ratio increases and the two peaks in the shedding frequency appear to merge into one peak, the value of which approaches 0.2. A zoomed view of power spectra for $G/D = 0.25$ is shown in Fig. 6(b)

and compared with the experimental data (Price et al., 2002), which demonstrate a good agreement. A wide range of shedding frequency with more energetic high-frequency harmonic is also observed from Fig. 6(a), which is attributed to the breaking down of primary vortices to small-scale energetic eddies downstream. The slope of the resolved inertial range appears to follow $-5/3$ power law correlation between the energy and the frequency. A summary of St data (considering prominent wake frequency) as a function of G/D obtained from the present simulations along with the experiments (Angrilli et al., 1982; Price et al., 2002) is presented, in Fig. 7. The LES at Re = 1440 agrees reasonably well with the available experimental data, where the Re was 1900. The validation illustrates that the present LES can be used to describe the evolution of shear layers shed from the cylinder under the influence of wall boundary layer.

The changes of flow features due to the presence of a wall are also reflected on the surface characteristics. The evolution of the mean skin friction ($\overline{C_f} = \overline{\tau_w}/0.5\rho U_\infty^2$, τ_w being the wall shear stress) along the wall for the three gap ratios is shown in Fig. 8. The separation and reattachment points along with the length of bubbles as marked in Fig. 5 are obtained from the distributions of $\overline{C_f}$. For $G/D = 0.25$, $\overline{C_f}$ becomes negative at $x/D = -2.58$ to -0.71, indicating an upstream separation, which is absent in the other two cases. The drop followed by a sharp rise of $\overline{C_f}$ upstream of $x/D = 0$ is due to the combination of wall proximity and flow acceleration beneath the cylinder. The peak value of $\overline{C_f}$ becomes maximum for this gap as the flow below the cylinder is under the maximum negative pressure. Downstream of the cylinder, $\overline{C_f}$ indicates an onset of separation at $x/D = 1.69$ with a large bubble length of $8.37D$, whereas the corresponding values are 1.06, $4.57D$ and 1.34, $3.04D$ for the gap ratio of 0.5 and 1.0, respectively. The appearance of a secondary bubble downstream for $G/D = 0.25$ and 0.5 is also reflected in the streamwise evolution of $\overline{C_f}$. When compared with the skin friction values evaluated from the correlation of turbulent flow, Fig. 8 further illustrates the relaxation and transition of flow near the wall. For $G/D = 1$, an overshoot of $\overline{C_f}$ is observed after reattachment of flow

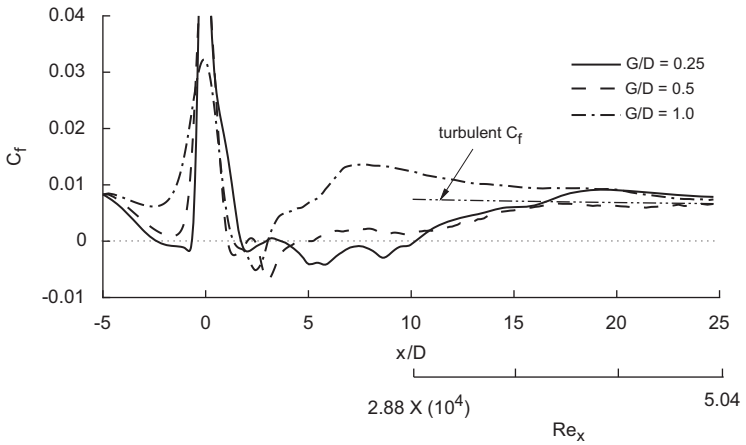

Fig. 8. Profiles of mean coefficient of friction (C_f) on the wall for different G/D ratios. Turbulent C_f profile obtained from the correlation $C_f = 0.058/Re_x^{1/5}$ is also superimposed.

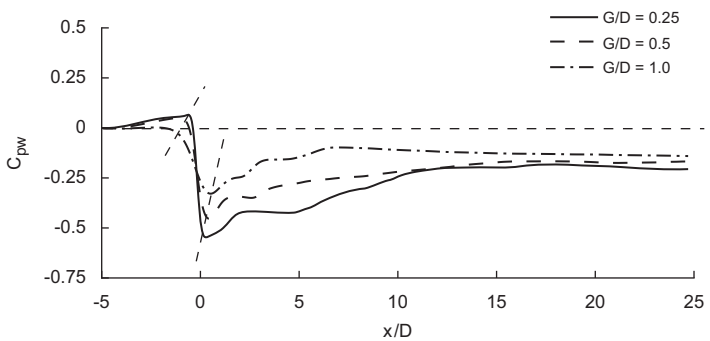

Fig. 9. Profiles of mean pressure coefficient on the wall (C_{pw}) for different G/D ratios. Minimum and maximum C_{pw} points are joined by dashed lines.

and it approaches the level of turbulent C_f downstream. For the other two cases, large regions of negative $\overline{C_f}$ are seen that slowly attain the level of turbulent C_f.

The distributions of time-averaged dimensionless pressure ($C_{pw} = (P_w - P_\infty)/0.5\rho U_\infty^2$, P_w being the wall pressure) on the wall are shown in Fig. 9 as a function of the gap ratio. There is a drop in pressure beneath the cylinder due to the flow acceleration with a plateau in C_{pw} that tends to recover downstream. With a decrease of G/D ratio, the magnitude of negative C_{pw} value increases with a large plateau illustrating a large separation region. Further to note that the location of minimum C_{pw} moves a little downstream, whereas the maximum C_{pw} moves upstream with the increase in gap ratio. The movements of these peaks (indicated by joining the locations of minimum and maximum C_{pw}) are attributed to the shift of front stagnation point towards the wall and the rear separation point along the shoulder of the cylinder as stated before. A similar trend was also found in the experiment of Choi and Lee (2000).

3.2. Instantaneous vortex dynamics

To visualize the vortex dynamics in proximity to a wall during the shedding cycle, the snapshots of iso-contours of spanwise vorticity (ω_z) and streamlines are presented in Figs. 10–15 for different gap ratios. These figures are drawn between a time period (T) of vortex shedding that has been calculated assuming the Strouhal frequency as 0.2. However, it should not be interpreted as St = 0.2 for all cases; indeed there is no such periodicity of the wake at all for a low gap ratio, $G/D = 0.25$ at Re = 1440. The Strouhal number as 0.2 represents an approximate average value over the range of G/D considered in the present study. A brief description of the vortex formation, its downstream convection, interaction with the boundary layer and breaking down to smaller eddies are described in this section.

Fig. 10 depicts the iso-contours of instantaneous ω_z ($t/T = 0.0$–0.8) along the mid-span section, indicating the flow behaviour for a small gap ratio, $G/D = 0.25$, which corresponds to $G/\delta = 0.6$ (δ being the boundary layer thickness at the location of cylinder without its presence). For $t/T = 0.0$, the outer shear layer shed from the cylinder is seen to curl up forming a vortex (denoted by A) over the inner shear layer, which is deflected away from the wall. The inner shear layer from the cylinder remains frozen for a long period of time and there is no apparent rollup. A strong pairing between the inner shear layer and the boundary layer is observed being of opposite sign that suppresses the shedding of the inner shear layer. This coupling also contributes to the lift-off of the boundary layer forming a separation bubble downstream of the cylinder. The boundary layer appears to roll up (denoted by B) beneath the inner shear layer. For the next few steps ($t/T = 0.2$–0.6), the inner shear layer is stretched further developing a Kármán-vortex sheet-like structure (denoted by C): one end of it remains attached to the cylinder to form a quasi-steady attached wake, while the other end engulfs the outer roll A. This roll of negative vorticity with a patch of positive vorticity convects downstream and breaks down to smaller eddies. The mutual interaction of the wall vortices with the shed vortices creates a remarkable difference in the wake dynamics: the trajectories of shed vortices cross each other and the final vertical position is opposite with respect to the unbounded case. Thus, the clockwise vortices shed from the upper side of the cylinder occupy the lower position, while the counterclockwise vortices shed from the inner side of the cylinder occupy the upper position in the sheet; a similar trend is reported by Zovatto and Pedrizzetti (2001). At $t/T = 0.8$, neither vortex A nor vortex B is identified downstream, but a negative vortex sheet appears that convects with a speed slower than the free-stream. These migrating vortices impart momentum to the wall boundary layer and the small-scale perturbations are observed near the wall and downstream of $x/D = 5$.

Instantaneous span-averaged vorticity at two time instants ($t/T = 0.4$ and 0.8) and the corresponding streamlines downstream of cylinder are shown in Fig. 11 for $G/D = 0.25$. The span-averaging removes the small-scale fluctuations and indicates the coherent structures. The span-averaged results also illustrate the coupling between the inner-side shed vortices and the wall vortices, the suppression of the shedding of inner shear layer and deflection of wake trajectory. A prominent feature of flow visualization with the span-averaging is the appearance of a wake sheet of negative vorticity downstream that has lost its discrete vortical structure. The roll of negative vortices from the upper shear layer merges with the boundary layer vortices and convects downstream before breakdown to form this wake sheet of the same-sign vorticity. The span-averaged streamlines indicate the appearance of a large separation bubble, unsteady in nature, downstream of the cylinder.

For $G/D = 0.5$ that corresponds to $G/\delta = 1.2$, both the inner and outer shear layers shed from the cylinder curl up in an almost alternating fashion producing two rolls (denoted by A and C), although lack of symmetry is evident at $t/T = 0$ as shown in Fig. 12. The lift-off of wall boundary layer occurs with a tongue-like vortex sheet that forms a roll denoted by B. However, this deflection of the boundary layer decreases, which in turn reduces the size of the downstream separation bubble as compared to the earlier. The curling of the shear layers also appears to form closer to the cylinder. As time progresses ($t/T = 0.2$–0.6), a rapid stretching of the inner shear layer is observed, forming an elongated vortex sheet, and its coupling with the wall boundary layer leads to the formation of a large negative roll as

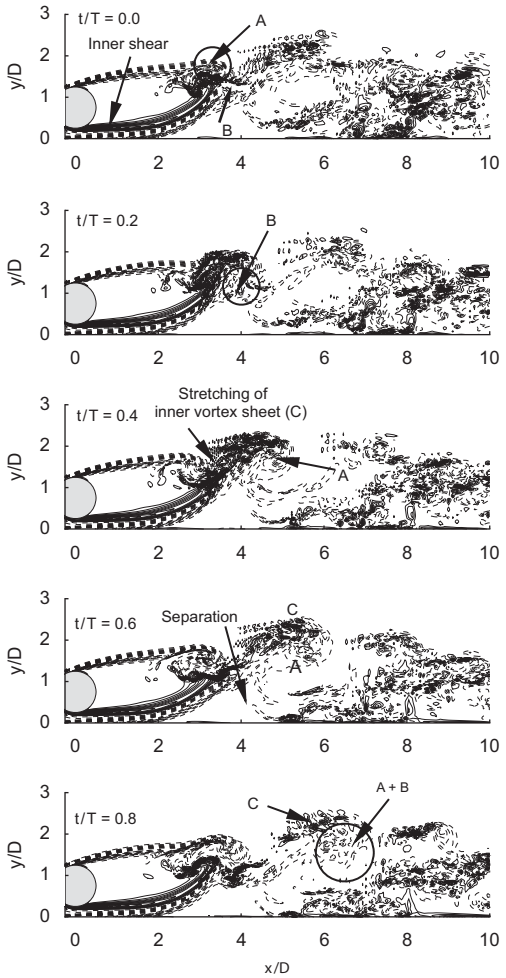

Fig. 10. Instantaneous ω_z contours for $G/D = 0.25$. Total 40 non-dimensional contours are considered in between -10 and $+10$. The negative vorticity is represented by the dotted line.

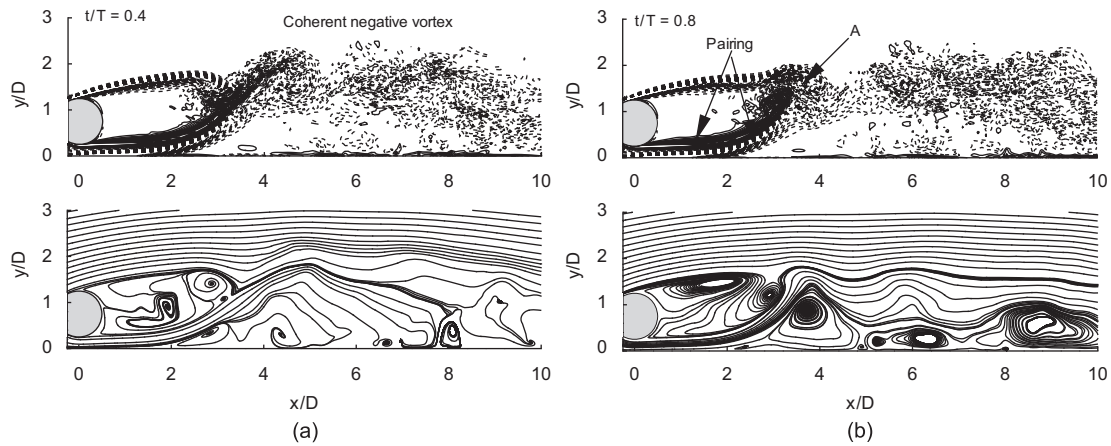

Fig. 11. Iso-contours of span-averaged ω_z and corresponding streamlines for $G/D = 0.25$. Total of 40 nondimensional contours are considered in between -5 and $+5$ for ω_z.

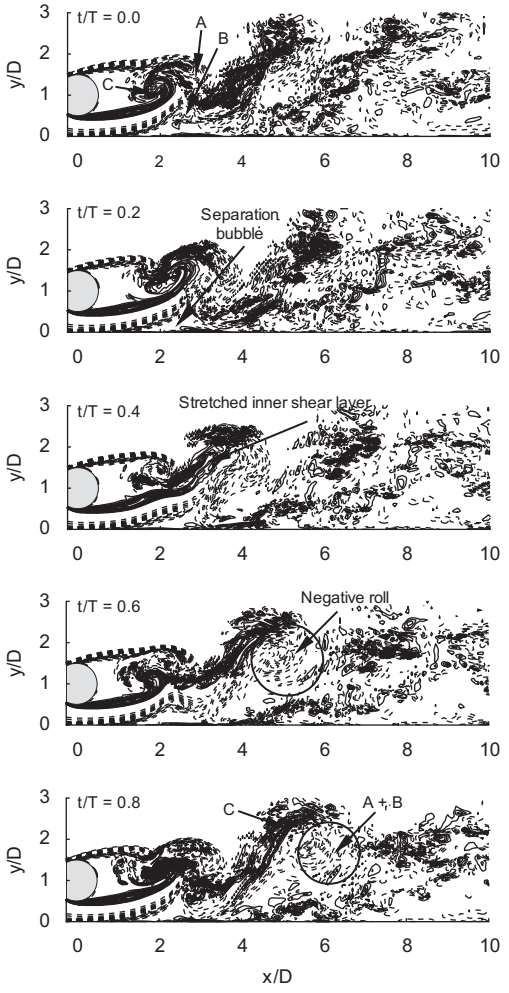

Fig. 12. Instantaneous ω_z contours for $G/D = 0.5$. For details refer to Fig. 10.

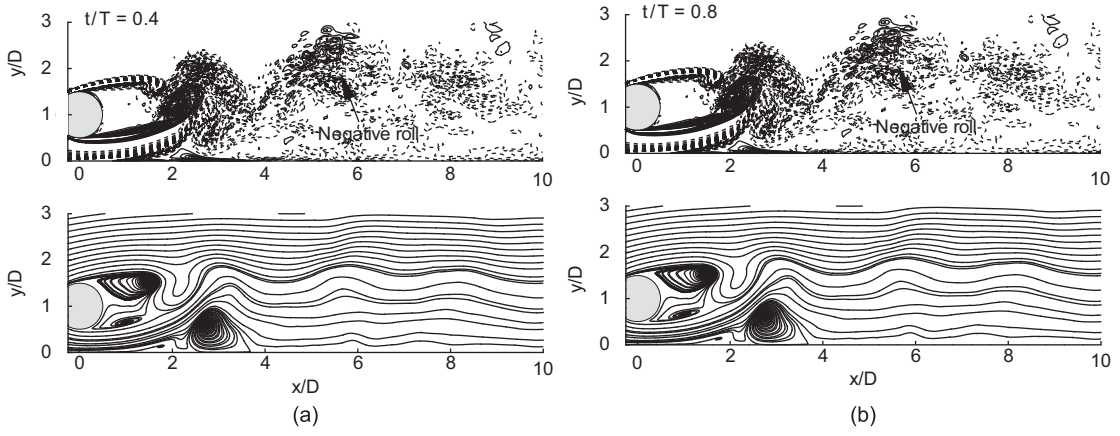

Fig. 13. Iso-contours of span-averaged ω_z and corresponding streamlines for $G/D = 0.5$. For details refer to Fig. 11.

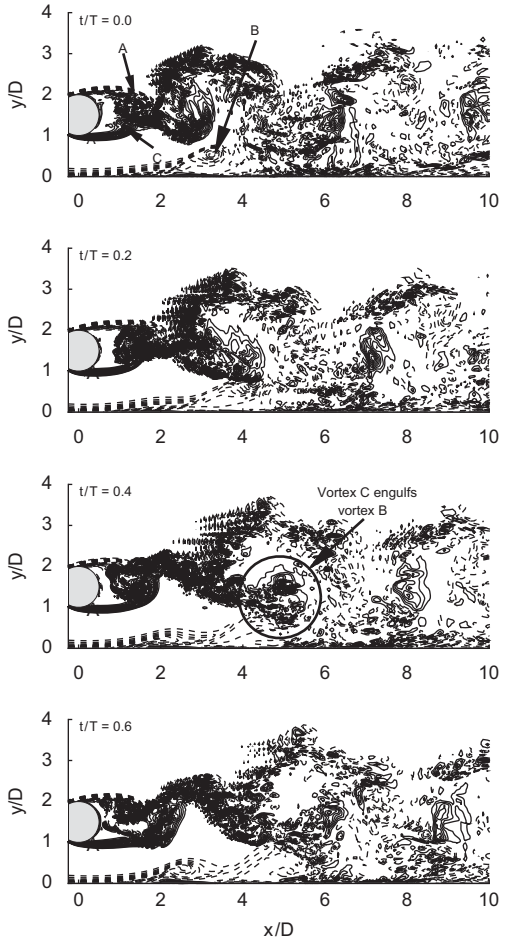

Fig. 14. Instantaneous ω_z contours for $G/D = 1.0$. For details refer to Fig. 10.

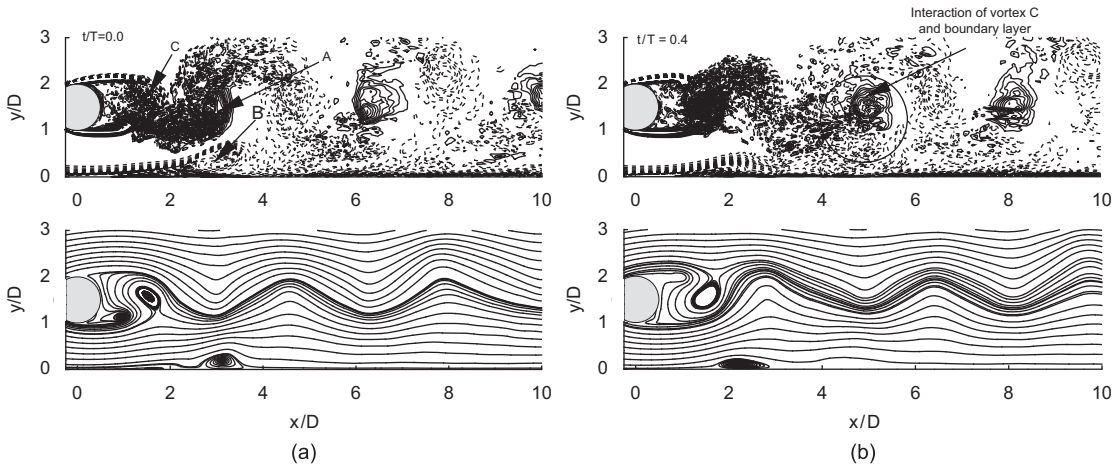

Fig. 15. Iso-contours of span-averaged ω_z and corresponding streamlines for $G/D = 1.0$. For details refer to Fig. 11.

before. The celerity of negative roll and positive vortex sheet appears marginally different: the positive vortex sheet stays above the negative roll. The stretching process is expected to decay the circulation of the wake vortex because of dissipation. The positive vortex sheet appears to interact with the boundary layer periodically and the perturbations of

the wall boundary layer downstream of $x/D = 5$ are higher in this case. The span-averaged results seen in Fig. 13 for $t/T = 0.4$ and 0.8 illustrate the similar flow visualization with alternating vortex shedding, stretching of the inner shear layer and the wall boundary layer, resulting in convection of a dominant negative vortex. Streamlines illustrate the appearance of downstream separation bubble, which is unsteady and coupled with vortex shedding from the cylinder in a periodic manner.

As the gap ratio increases, the snapshots of spanwise vorticity (Fig. 14 for $G/D = 1.0$ that corresponds to $G/\delta = 2.4$) over a time period of vortex shedding illustrates that the cylinder behaves closer to an isolated cylinder with an alternate vortex shedding. However, this shedding of Kármán vortex, particularly the inner shear layer and the associated positive vortex rolls (denoted by C), influences the wall boundary layer in a different fashion. The excitation of the boundary layer downstream of $x/D = 5$ appears to be substantial by this positive migrating rolls. In detail, downstream of the cylinder a negative vortex from the wall boundary layer eventually elongates (denoted by B), forming a vortex sheet that is seen to be engulfed by the positive convective vortex roll (Fig. 14, $t/T = 0.6$). This creates an unsteady bubble beneath the negative vortex sheet, the periodicity of which appears to be the same as that of the vortex shedding. The span-averaged vorticity (Fig. 15) illustrates the coherent vortex rolls depicting the dynamics as explained before. It explains a three-layer structure, which is slightly deflected away from the wall, where the inner shear layer periodically interacts with the wall boundary layer. The rollup of boundary layer forming small-scale eddies because of excitation of the convective coherent vortices is apparent downstream of $x/D = 5$. The corresponding streamlines also suggest the formation of a small unsteady bubble downstream of the cylinder.

To validate the wake dynamics evaluated in the presented LES, the iso-contours of spanwise vorticity (ω_z) are compared in Fig. 16 to the corresponding experiment (Price et al., 2002) for $G/D = 0.25$ and 0.5. The wake–boundary layer interactions, formation of separation bubbles both upstream and downstream of the cylinder, stretching of shear layers shed from the cylinder, rollup and then breaking down into smaller eddies are well represented. The numerical visualization of instantaneous flow field illustrates a close resemblance with the experimental observations (Price et al., 2002) in terms of vortex dynamics and flow structures.

Figs. 17 and 18 illustrate the overall trajectory of peak vorticity and the variation of vortex peak values along the streamwise direction for $G/D = 0.5$ and 1.0. Three vortices emanating from the outer shear layer, the inner shear layer and the wall boundary layer are traced to reveal the vortex motion. For $G/D = 0.5$, vortices from the inner shear layer and the wall boundary layer travel in an almost parallel trajectory owing to the coupling between them (Fig. 17(a)) and move in the wall-normal direction behind the cylinder ($x/D < 3.0$). The outer shear layer vortices move almost parallel to the wall. Near $x/D = 4.5$, a strong mutual interaction between vortices is reflected by the cross-over of trajectories of the shed vortices emerging a prominent negative vortex that travels downstream and remains almost parallel to the wall. Fig. 17(b) indicates that the peak values of the shed vortices decay at a higher rate than that of the wall vortices near the cylinder ($x/D < 4$). Furthermore, the wall vortices decay rapidly in the vicinity of the cylinder and at a slower rate downstream of $x/D = 4$. This is attributed to the breakdown of the larger-scale vortex to the random small-scale eddies resulting in a decrease of the magnitudes of lower frequency and the increase of higher frequency energy-content eddies. It should be further noted that the inner shear layer and the wall boundary layer do not cancel each other behind the cylinder, although of different signs of vorticity. This supports the experimental observation of Price et al. (2002), while it contradicts the suggestion of Grass et al. (1984) and Taniguchi and Miyakoshi (1990).

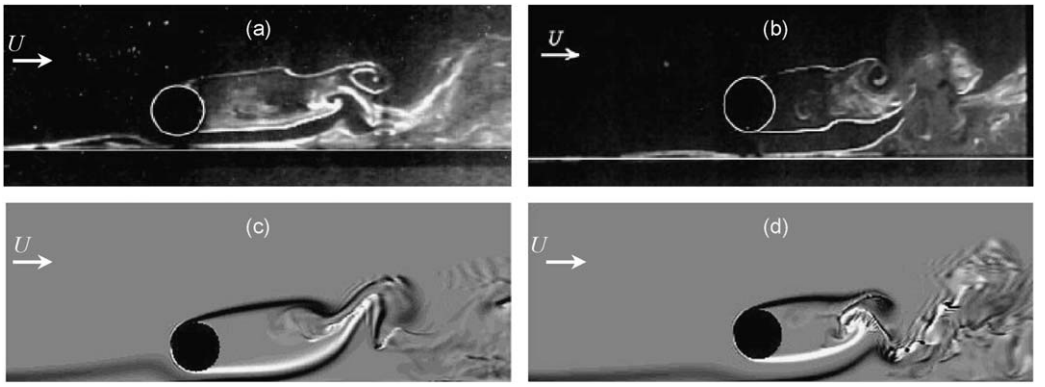

Fig. 16. Instantaneous spanwise vorticity (ω_Z): (a) and (b) experiment at Re = 1900 (Price et al., 2002); (c) and (d) present LES at Re = 1440. (a) and (c) $G/D = 0.25$; (b) and (d) $G/D = 0.5$.

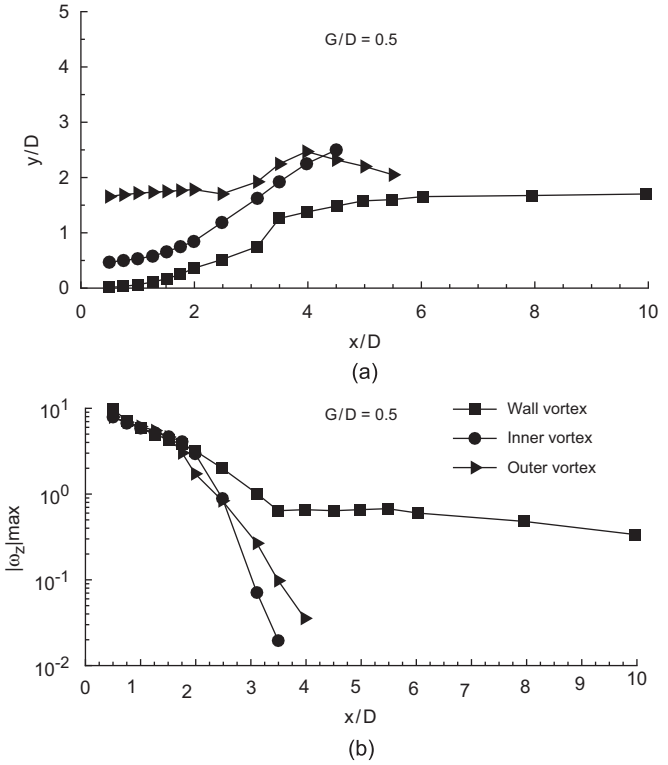

Fig. 17. (a) Trajectory of vortex peak and (b) variation of vortex peak values for $G/D = 0.5$ and $\mathrm{Re} = 1440$.

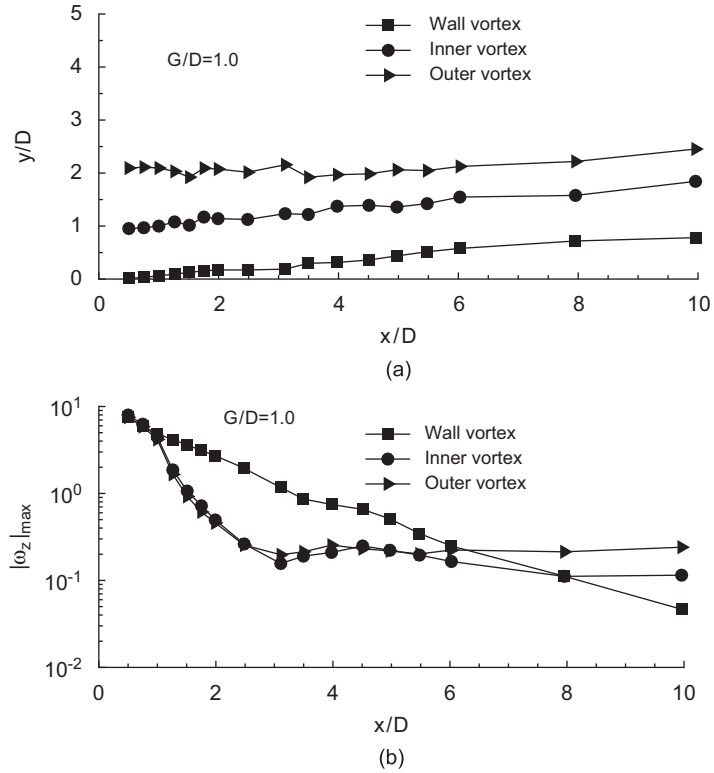

Fig. 18. (a) Trajectory of vortex peak and (b) variation of vortex peak values for $G/D = 1.0$ and $\mathrm{Re} = 1440$.

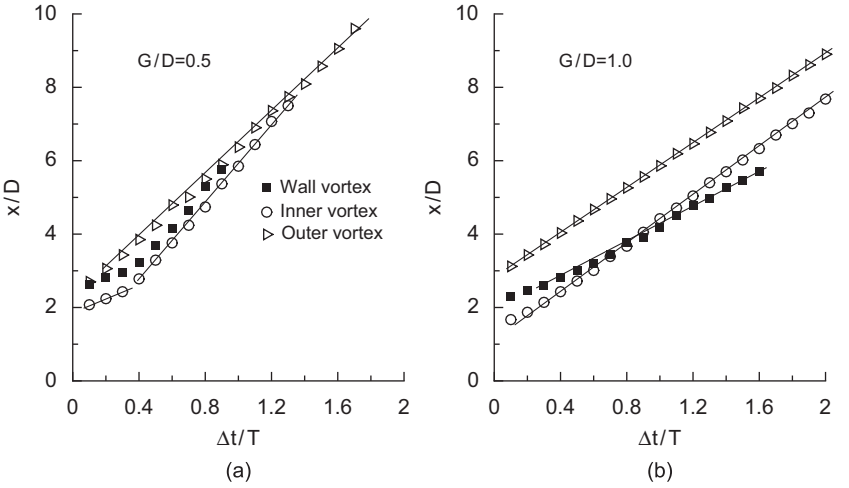

Fig. 19. Time history of spanwise vorticity peak along the streamwise direction for Re = 1440; (a) $G/D = 0.5$ and (b) $G/D = 1.0$.

As the cylinder is moved away from the wall ($G/D = 1$), the outer- and inner-side-shed vortices along with the wall vortex can be separately identified far downstream of the cylinder (Fig. 18). The trajectories of vortex peak illustrate that the vortices migrate parallel to each other. In this case, the effect of boundary layer is minimum and so both the outer- and inner-shear layers roll up to produce almost identical vortices. Further, the outer and inner vortices have the same decay profile (rapidly in the vicinity of the cylinder and at a slower rate downstream of $x/D = 4$), which mean that the interaction between them is a mutual process. The wall vortex appears to decay continuously, but at a slower rate behind the cylinder.

Fig. 19 depicts the streamwise locations of the vortex peak with time for $G/D = 0.5$ and 1.0. The slope of the curve gives the vortex celerity. For $G/D = 0.5$, the inner vortex travels with a velocity of $0.38U_\infty$ up to $t/T = 0.2$ and then suddenly accelerates due to attraction of outer vortices and travels with a speed of U_∞. This slower celerity of the inner vortex at the beginning is attributed to the wall effect imposing on alternating vortex formation near the base region. The outer vortex travels with a constant speed of $0.9U_\infty$. The wall vortex travels almost with the same celerity of the lower vortex illustrating a pairing between them as explained earlier. Time history of vortex celerity changes for $G/D = 1.0$, which depicts that the wall vortex travels at a speed of $0.52U_\infty$, while the outer- and inner-vortex travel at speeds of $0.65U_\infty$ and $0.7U_\infty$, respectively. The speeds of the outer- and inner-vortex come close to the speed of the Kármán vortex from an isolated cylinder [$0.78U_\infty$, Lin et al. (1995)] as the gap ratio increases.

The iso-surface of the spanwise component of instantaneous vorticity for different gap ratios is depicted in Fig. 20 to visualize the 3-D flow structures and internal growth mechanism of shear layers after instability in proximity to a wall. For a low gap ratio ($G/D = 0.25$), the outer shear layer shed from the cylinder appears to remain laminar up to $x/D = 2.5$ and then the shear layer instability sets in with the appearance of longitudinal streaks that quickly break down to turbulent flow downstream. To distinguish between the inner shear layer, which is of positive vorticity, and the boundary layer of negative vorticity, different colours are used. As stated earlier, the boundary layer in this case is highly deflected away from the wall, producing a large separation region due to its strong coupling with the inner shear layer. It is commonly accepted that a separated laminar layer is inherently unstable and promotes the growth of disturbances. A rapid growth of disturbances appears after the point of separation that breaks down to random structures near $x/D = 3$. The flow is turbulent downstream with the appearance of small-scale, higher frequency energy-content eddies and loss of coherent structures. Thus, the generation of turbulence is prominent away from the wall, leaving a relatively calm near-wall because of the detached layer.

With increase of the G/D ratio the effect of wall proximity is decreased and the breakdown of both the outer and inner shear layers occurs relatively closer to the cylinder. The flow tends to retain its coherent structures with the appearance of spanwise small-scale eddies. Further, to note that the defection of the boundary layer is inhibited as the gap ratio is increased. For $G/D = 1$, a thin separation bubble is observed as seen in Fig. 5 and the boundary layer behaves almost like an attached layer. In this case, the receptivity to external disturbance is very prominent near the wall with the appearance of longitudinal streaky structures. The perturbations created by the turbulent shear layers are

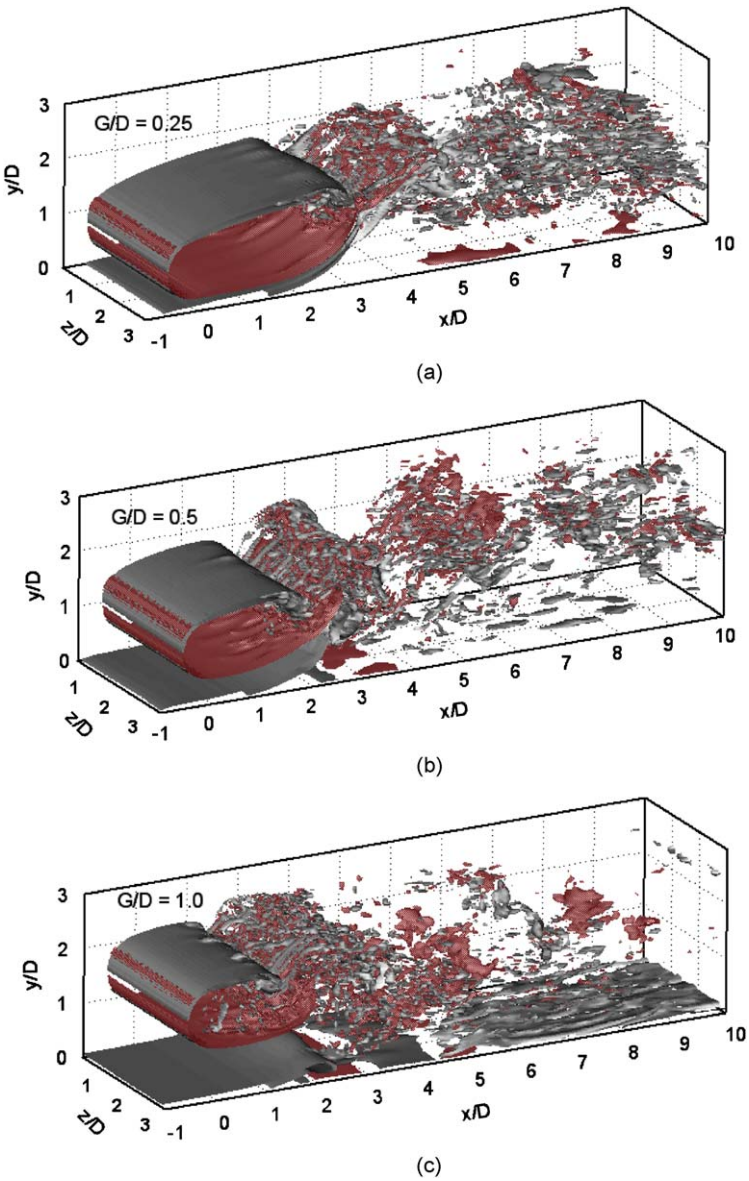

Fig. 20. Iso-surfaces of spanwise vorticity ($\omega_z = \pm 2.0$) for (a) $G/D = 0.25$, (b) $G/D = 0.5$ and (c) $G/D = 1.0$.

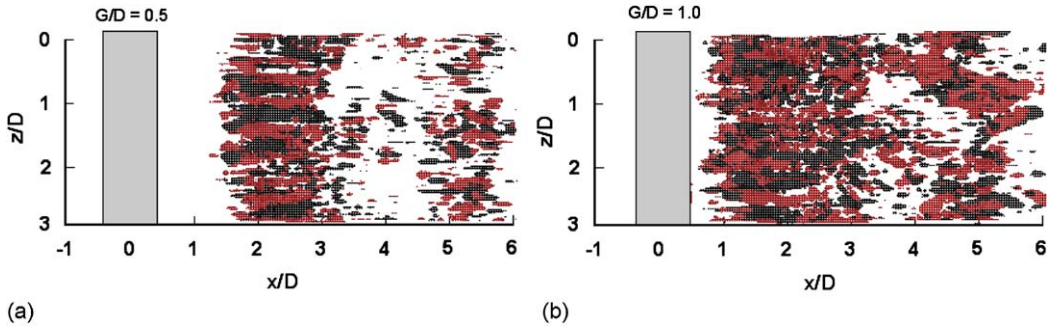

Fig. 21. Iso-surfaces of streamwise vorticity ($\omega_x = \pm 4.0$) for $G/D = 0.5$ and $G/D = 1.0$.

amplified near the wall due to the inflexional layer, and then the nonlinear interactions of vortex stretching process create these streaks, which are characteristics of turbulent flow.

Fig. 21 illustrates the iso-surface of ω_x for $G/D = 0.5$ and 1.0 at the same time instant. The figure illustrates the instability of the shear layers with the formation of streaky structures having a spanwise wavelength of $0.5D$ and this instability occurs earlier for a larger gap ratio. The streaks become three-dimensional and break down to small-scale eddies downstream. These small-scale vortices appear to overshadow the main vortices and the flow turns out to be turbulent. It should be noted that Mansy et al. (1994) have given an empirical formula for the wavelength of the streamwise structures in the near wake as $20Re^{-0.5}D$ using the data in the range of $300 \leq \mathrm{Re} \leq 1200$. This empirical relation estimates a wavelength of $0.52D$ at $\mathrm{Re} = 1440$, which is very close to the value of wavelength obtained from the present simulation. Hence, the mode of instability of the shear layer in proximity to a wall would be close to that of the unbounded condition, although the breakdown and generation of the small-scale eddies would differ as these are sensitive to external perturbations.

3.3. Turbulence statistics

To understand the relative effects of G/D ratio on the wake and boundary layer interactions, the iso-contours of Reynolds normal ($\overline{u'u'}/U_\infty^2$) and shear ($\overline{u'v'}/U_\infty^2$) stress behind the circular cylinder are presented in Fig. 22(a) and (b) for the three gap ratios, $G/D = 0.25$, 0.5 and 1.0. A few selected streamlines representative of trajectories of the shear layers and the approaching boundary layer are superimposed to illustrate the correspondence between the mean flow and the stresses.

In unbounded condition, the contours of time-averaged turbulent stresses of flow past a cylinder are found to be symmetric about the centreline with a double-peak feature. The symmetry in normal and shear stress distributions is lost completely as the cylinder is placed close to a wall, $G/D = 0.25$ corresponding to $G/\delta = 0.6$. In this case, the stresses appear to develop towards the end of the recirculation region, indicating a delay in transition because of frozen shear layers. The breakdown of the shear layers is reflected by the enhanced stress levels near $x/D = 3$. The deflection of the boundary layer due to the pairing with the inner shear layer, its stretching and convection over the downstream

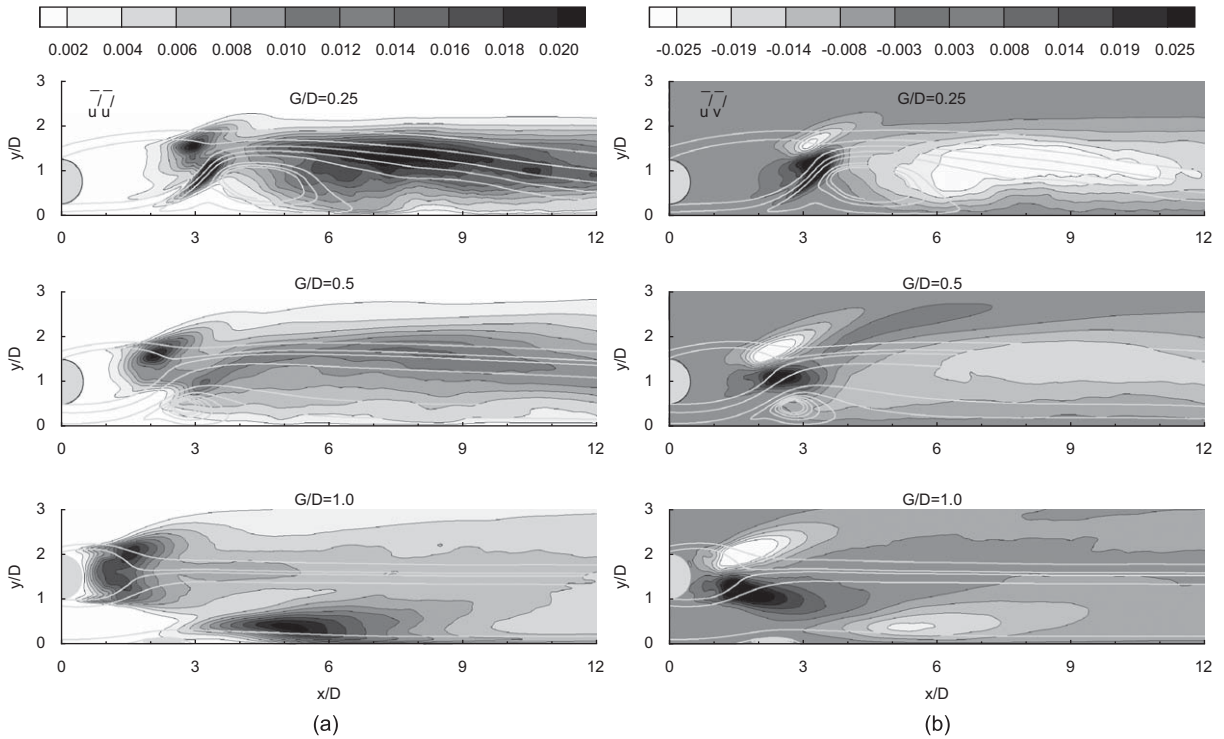

Fig. 22. Iso-contours of (a) Reynolds normal stress and (b) Reynolds shear stress for $G/D = 0.25$, 0.5 and 1.0.

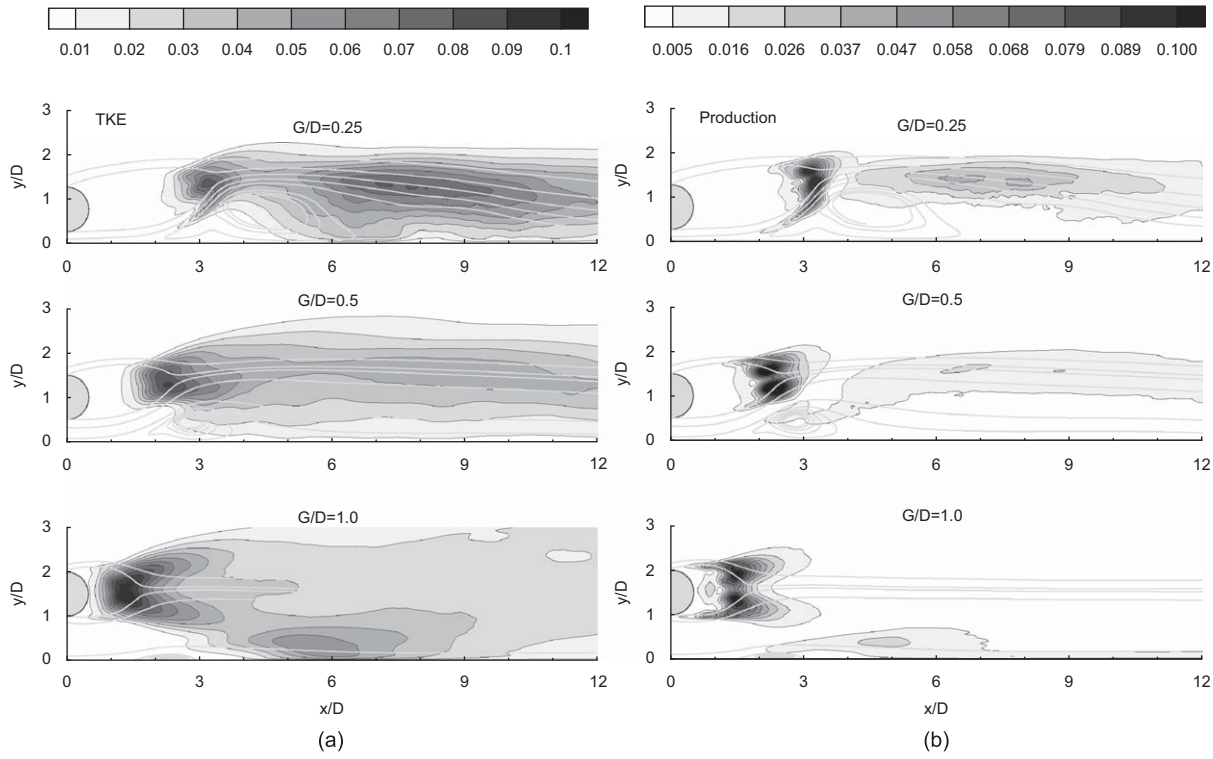

Fig. 23. Iso-contours of (a) turbulent kinetic energy and (b) production for $G/D = 0.25$, 0.5 and 1.0.

bubble are resolved in the evolution of enhanced stresses. In downstream, high values of the normal stresses occur away from the wall along the trajectories of the shear layer. However, it should be noted that shear stress is not maximum on the separating streamlines: the maximum value occurs a bit away where the velocity gradient is maximum. For $G/D = 0.5$ or $G/\delta = 1.2$, the enhancement of turbulent stresses occurs along the trajectories of the shear layer, leaving a relatively low value of stresses near the wall. It is interesting to note that the turbulent stresses appear to re-establish the symmetry with the double-peak features as the cylinder is placed relatively away from the wall at $G/D = 1$, which corresponds to $G/\delta = 2.4$. Here, the transition of the shear layers occurs much earlier with the formation of rolls closer to the cylinder at $x/D = 1.5$. In this case, the enhancement of both the normal and shear stresses is found to occur near the wall, which initiates at the reattachment point of the bubble and becomes maximum at $x/D = 5.25$. This illustrates the excitation of boundary layer by the convective wake.

In addition to Reynolds stresses, the evolution of TKE along with its production [$P_{\mathrm{TKE}} = -\overline{u_i' u_j'}(\partial \bar{u}_i/\partial x_j)$] is shown in Fig. 23 to highlight the influence of G/D. As expected, the enhancement of turbulence occurs along the trajectories of the shear layers, leaving a relatively calm near-wall region for low gap ratios (G/D up to 0.5), which is very consistent with the distribution of the normal stresses. This is attributed to the strong coupling between the approaching boundary layer and the inner shear layer, leading to a rapid growth of disturbances with the appearance of small-scale eddies in regions away from the wall: an example of mutual interactions between the boundary layer and the shear layer. In these cases, the production occurs in the same locations of high TKE, where the turbulence extracts work from the mean flow. This happens in regions of high turbulent stress and high spatial velocity gradient, aligned in the same direction. Thus, the high production along the path of the wake is due to the coexistence of turbulent stress and shear in the wake fluid. The delay in transition of shear layers following breakdown is also reflected in iso-contours of TKE and production. For a large gap ratio ($G/D = 1.0$), the cylinder remains well outside the boundary layer and the wake dynamics emerges to be different from that of the other two cases, which has been reflected in the TKE and production contours. In this case, the high TKE and production are not confined along the path of the shear layers; rather, the augmentation is migrated towards the wall. The inner shear layer shed from the cylinder perturbs the inflexional boundary layer generating higher frequency energy-content eddies and the turbulence: an example of receptivity of external disturbances. The high production near the surface can be considered as the combined effect of a local

concentration of vorticity and a growing level of turbulence in the boundary layer. The almost symmetrical distribution of TKE and production behind the cylinder further confirm that the effect of boundary layer on the shear layers is minimal in this case, and the shear layers roll close to the cylinder.

4. Conclusions

Large-eddy simulations of flow past a circular cylinder in the vicinity of a wall have been carried out for three different gap ratios at a Reynolds number in the shear layer transition region, following the experiment of Price et al. (2002). An attempt is made to describe the physics of flow involving the nonlinear interactions of shear layers shed from the cylinder and the approaching boundary layer. The present LES reveals that the G/D ratio has a strong influence on shear layer instability, modification of wake dynamics apart from its coherent structure and small-scale motion.

When the inner shear layer lies within the boundary layer ($G \leq \delta$), a strong coupling between the inner shear layer and the approaching boundary layer is observed, with suppression of vortex shedding and stretching of the shear layers. Furthermore, the front stagnation point shifts towards the wall, generating an upward lift that deflects the boundary layer, resulting in a relatively large separation behind the cylinder. The mutual interactions of the wall vortices with the shed vortices create a remarkable difference in the wake dynamics: trajectories of shed vortices cross each other and an inversion on the position of vortices occurs with respect to the unbounded case. The coupling between the inner shear layer and the boundary layer also delays the shear layer instability and the appearance of a spanwise wavy structure, which becomes three-dimensional and breaks down at the end of the recirculation region. In this case, the generation of turbulence is mainly due to shear in the wake fluid, illustrating a highly active outer region along the wake trajectory and a relatively calm near-wall.

The wake dynamics appears to be different as the cylinder is kept outside the boundary layer ($G = 2.4\delta$). In this case, the shear layers and the boundary layer can be separately identified. The breakdown of the shear layers occurs relatively closer to the cylinder and the wake tends to retain its coherent structures with the appearance of small-scale eddies. The Strouhal frequency becomes close to 0.2, although asymmetry in the wake shape is observed. What is interesting is that the vortices shed from the cylinder inject momentum to the boundary layer during their convection, triggering its transition. Thus, the generation of turbulence does not occur along the wake trajectories; rather, the augmentation of turbulent stresses is found near the wall, initiating at the reattachment point of the downstream bubble: an example of receptivity of external disturbances. The appearance of streaky structures near the wall is also evidence of transitional boundary layer. Thus, it is worthwhile to note the differences in response of the boundary layer close to a migrating wake as the gap ratio changes.

References

Angrilli, F., Bergamaschi, S., Cossalter, V., 1982. Investigation of wall induced modifications to vortex shedding from a circular cylinder. ASME Journal of Fluids Engineering 104, 518–522.

Bearman, P.W., Zdravkovich, M.M., 1978. Flow around a circular cylinder near a plane boundary. Journal of Fluid Mechanics 89, 33–47.

Beaudan, P., Moin, P., 1994. Numerical experiments on the flow past a circular cylinder at sub-critical Reynolds number. Report No. TF-62, Department of Mechanical Engineering, Stanford University.

Berger, E., Willie, R., 1972. Periodic flow phenomena. Annual Review of Fluid Mechanics 4, 313–340.

Buresti, G., Lanciotti, A., 1979. Vortex shedding from smooth and roughened cylinders in cross-flow near a plane surface. The Aeronautical Quarterly 30, 305–321.

Choi, J.H., Lee, S.J., 2000. Ground effect of flow around an elliptic cylinder in a turbulent boundary layer. Journal of Fluids and Structures 14, 697–709.

Dipankar, A., Sengupta, T.K., 2005. Flow past a circular cylinder in the vicinity of a plane wall. Journal of Fluids and Structures 20, 403–423.

Drikakis, D., 2003. Advances in turbulent flow computations using high-resolution methods. Progress in Aerospace Sciences 39, 405–424.

Fadlun, E.A., Verzicco, R., Orlandi, P., Mohd.-Yusof, J., 2000. Combined immersed boundary finite difference methods for three dimensional complex flow simulations. Journal of Computational Physics 161, 35–60.

Germano, M., Piomelli, U., Moin, P., Cabot, W.H., 1991. A dynamic subgrid-scale eddy viscosity model. Physics of Fluids A 3, 1760–1765.

Grass, A.J., Raven, P.W.J., Stuart, R.J., Bray, J.A., 1984. The influence of boundary layer velocity gradients and bed proximity on vortex shedding from free spanning pipelines. ASME Journal of Energy Resources Technology 106, 70–78.

Jacobs, R.G., Durbin, P.A., 2001. Simulations of bypass transition. Journal of Fluid Mechanics 428, 185–212.
Kravchenko, A.G., Moin, P., 2000. Numerical studies of flow over a circular cylinder at $Re_D = 3900$. Physics of Fluids 12, 403–417.
Lei, C., Cheng, L., Kavanagh, K., 1999. Re-examination of the effect of a plane boundary on force and vortex shedding of a circular cylinder. Journal of Wind Engineering and Industrial Aerodynamics 80, 263–286.
Lilly, D.K., 1992. A proposed modification of the Germano subgrid-scale closure method. Physics of Fluids A 4, 633–635.
Lin, J.C., Towfighi, J., Rockwell, D., 1995. Instantaneous structure of the near-wake of a circular cylinder: on the effect of Reynolds number. Journal of Fluids and Structures 9, 409–418.
Liou, T.M., Chen, S.H., Hwang, P.W., 2002. Large eddy simulation of turbulent wake behind a square cylinder with a nearby wall. ASME Journal of Fluids Engineering 124, 81–90.
Lourenco, L.M., Shih, C., Characteristics of the plane turbulent near wake of a circular cylinder, a particle image velocimetry study, data taken from Ma et al. (2000).
Ma, X., Karamanos, G.-S., Karniadakis, G.E., 2000. Dynamics and low-dimensionality of a turbulent near wake. Journal of Fluid Mechanics 410, 29–65.
Mansy, H., Yang, P.-M., Williams, D., 1994. Quantitative measurements of three-dimensional structures in the wake of a circular cylinder. Journal of Fluid Mechanics 270, 227–296.
Mittal, R., Balachandar, S., 1995. Effect of three-dimensionality on the lift and drag of no two-dimensional cylinders. Physics of Fluids 7, 1841–1865.
Mittal, R., Moin, P., 1997. Suitability of upwind-biased finite-difference schemes for large-eddy simulation of turbulent flows. AIAA Journal 35, 1415–1417.
Morinishi, Y., Lund, T.S., Vasilyev, O.V., Moin, P., 1998. Fully conservative higher order finite difference schemes for incompressible flow. Journal of Computational Physics 143, 90–124.
Muldoon, F., Acharya, S., 2005. Mass conservation in immersed boundary method. In: Proceedings of FEDSM 2005, FEDSM, 77301, pp. 1–9.
Norberg, C., 1994. An experimental investigation of the flow around a circular cylinder: influence of aspect ratio. Journal of Fluid Mechanics 258, 287–316.
Ong, L., Wallace, J., 1996. The velocity field of the turbulent very near wake of a circular cylinder. Experiments in Fluids 20, 441–453.
Orlanski, I., 1976. Simple boundary condition for unbounded hyperbolic flows. Journal of Computational Physics 21, 251–269.
Ovchinnikov, V., Piomelli, U., Choudhari, M.M., 2006. Numerical simulations of boundary-layer transition induced by a cylinder wake. Journal of Fluid Mechanics 547, 413–441.
Price, S.J., Sumner, D., Smith, J.G., Leong, K., Paidoussis, M.P., 2002. Flow visualization around a circular cylinder near to a plane wall. Journal of Fluids and Structures 16, 175–191.
Roshko, A., 1961. Experiments on the flow past a circular cylinder at very high Reynolds number. Journal of Fluid Mechanics 10, 345–356.
Sarkar, Sudipto, Sarkar, S., 2007. Immersed boundary method for simulating complex flows. In: Proceedings of ICFD'07, University of Reading, UK.
Sarkar, S., Sarkar, Sudipto, 2007. Large-eddy simulations of cylinder boundary layer interactions. In: Proceedings of ACFD 7, pp. 1349–1360.
Sarkar, S., Voke, P.R., 2006. Large-eddy simulation of unsteady surface pressure on a LP turbine blade due to interactions of passing wakes and inflexional boundary layer. ASME Journal of Turbomachinery 128, 221–231.
Sarkar, S., 2007. The effects of passing wakes on a separating boundary layer along a low-pressure turbine blade through large-eddy simulation. IMechE Journal of Power Energy 221, 551–564.
Sarkar, S., 2008. Identification of flow structures on a LP turbine blade due to periodic passing wakes. ASME Journal of Fluids Engineering 130, 1–10.
Schlichting, H., 1979g. Boundary-Layer Theory, 7th ed. McGraw-Hill.
Taneda, S., 1965. Experimental investigation of vortex streets. Journal of the Physics Society of Japan 20, 1714–1721.
Taniguchi, S., Miyakoshi, K., 1990i. Fluctuating fluid forces acting on a circular cylinder and interference with a plane wall. Experiments in Fluids 9, 197–204.
Vada, T., Nestegard, A., Skomedal, N., 1989. Simulation of viscous flow around a circular cylinder in the boundary layer near a wall. Journal of Fluids and Structures 3, 579–594.
Williamson, C.H.K., 1996. Vortex dynamics in the cylinder wake. Annual Review of Fluid Mechanics 28, 477–539.
Zdravkovich, M.M., 1985. Forces on a circular cylinder near a plane wall. Applied Ocean Research 7, 197–201.
Zhang, S.L., 1997. GPBi-CG: generalized product-type methods based On Bi-CG for solving nonsymmetric linear systems. SIAM Journal of Scientific Computing 18, 537–551.
Zovatto, L., Pedrizzetti, G., 2001. Flow about a circular cylinder between parallel walls. Journal of Fluid Mechanics 440, 1–25.